RSC Advances

PAPER

View Article Online
View Journal | View Issue

Open Access Article. Published on 22 December 2020. Downloaded on 1/15/2026 2:18:28 PM.
This article is licensed under a Creative Commons Attribution-NonCommercial 3.0 Unported Licence.

Check for updates

Cite this: *RSC Adv.*, 2020, **10**, 45139

Dielectric properties of poly-(3-octylthiophene) thin films mixed with oleic acid capped cadmium selenide nanoparticles

Mohsen Elain Hajlaoui,[a] Aida Benchaabane,[bc] Zied Benhamed,[c] Nourdine Mahdhi,[d] Ahmed A. Al-Tabbakh[e] and Fayçal Kouki[c]

Received 29th October 2020
Accepted 14th December 2020

DOI: 10.1039/d0ra09236c

rsc.li/rsc-advances

Hybrid heterojunction thin films, based on poly-(3-octylthiophene) (P3OT) polymer and oleic acid (OA)-capped cadmium selenide (CdSe) nanoparticles (NPs) are prepared by a spin-coating method. The structural and morphological properties of the CdSe NPs and of the hybrid thin films are investigated. The results of the dielectric characterization show that conductivity of the hybrid thin films is dependent on frequency and CdSe NP concentration. The Nyquist plots of the impedance characteristics of the layers exhibit circular features irrespective of the NP concentration. The dependence of the dielectric permittivity on frequency and CdSe NP concentration are studied.

Introduction

Bulk heterojunctions (BHJs) of nano-composite materials have received extensive attention from the scientific and technological communities for being potential alternatives to conventional heterojunctions in multiple technological applications.[1–5] BHJs are currently used in optoelectronics,[6–10] radiation detection and photodetection systems,[11,12] dielectrics and photovoltaic devices,[13,14] biology and medicine.[15–18] In hybrid photovoltaic devices, the polymer and the inorganic components offer additional complementary advantages owing to their low-cost manufacturing processes, flexibility, reproducibility, and versatile functionalities.[19–21] In hybrid composite devices, NPs play an important role in improving the optical and electrical properties of the devices.[22] Numerous studies have been conducted to investigate the influence, on the charge transfer process, of incorporating nanoparticles into the polymer matrix (*i.e.* the trapping and de-trapping of charges,[23–25] the formation of conductive filament paths, and the charge transfer between the NPs and the organic materials).[26–28]

Furthermore, the efficiency of charge generation may be enhanced by improving the mixing quality of the polymer/nanoparticles thus providing an efficient exciton dissociation at the donor/acceptor interface. Owing to the extended path of the donor/acceptor interface, hybrid composite devices hold the advantage over the traditional multilayer models.[29] However, the selection of appropriate inorganic semiconductor NPs for certain applications is still debated in the literature. Zinc selenide (ZnSe), cadmium sulfide (CdS), and other inorganic semiconductors are, nevertheless, suitable candidate materials for optoelectronic applications due to an improved efficiency of the functioning nano-composite devices.[30–35]

CdSe NPs are known to offer advantageous optoelectronic properties compared with other counterparts.[36–38] One way of improving the synthesis of the NPs is by using surface ligands to facilitate charge transfer between the phases.[39,40] Several capping agents were used in the synthesis of CdSe NPs such as TOPO, octanethiol, EtPO, TBPO, Pip3PO, and Pyrr3PO.[41] Apart from these materials, oleic acid (OA) can be used as a suitable capping agent with CdSe quantum dots (CdSe QD) to largely increase the QD loading and suppress the recombination of the separated charges.[42,43]

The highest efficiency for such hybrid device was obtained with CdSe NPs and polythiophene.[44,45] It is worth mentioning that the morphologies and distribution of the NPs in the polymer matrix represent important parameters influencing the optical and electrical properties, and thus the photovoltaic performances of the device.[46]

Previously, we have shown that the incorporation of oleic acid-capped CdSe NPs into a conducting host of poly(3-octylthiophene) (P3OT) matrix strongly affects the fluorescence of the hybrid nano-composite system and the photovoltaic performances of the P3OT:wt% OA-capped CdSe bulk heterojunction. In the present work, we study the concentration effect of the OA-capped CdSe NPs on the structural and dielectric properties of the P3OT:OA-capped CdSe composite thin

[a]*Institut Supérieur de Technologie Médicale, Université Tunis El-Manar, 1003 Tunis, Tunisia*

[b]*Laboratoire Matériaux Avancés et Phénomènes Quantiques, Faculté des Sciences de Tunis El Manar, Université Tunis El-Manar, Campus Universitaire, 2092 Tunis, Tunisia*

[c]*Ecole d'aviation de Borj El Amri, route Mjez El Beb, 1142 Tunis, Tunisia*

[d]*Laboratoire Matériaux, Organisation et Propriétés, Université de Tunis El Manar, Tunis 2092, Tunisia*

[e]*Department of Physics, College of Science, Al-Nahrain University, Baghdad, Iraq*

Open Access Article. Published on 22 December 2020. Downloaded on 1/15/2026 2:18:28 PM.
This article is licensed under a Creative Commons Attribution-NonCommercial 3.0 Unported Licence.

film. We used impedance spectroscopy to characterize the synthesized heterojunction materials. Then, we investigated the charge transport mechanism involved in ac conductivity.

Experimental

The polymer matrix used in this work is poly(3-octylthiophene) (P3OT) having a purity of 99% (procured from Sigma-Aldrich, Germany). The OA-capped CdSe NPs were prepared from a 1 : 1 mixture of cadmium acetate and OA in diphenyl-ether following the same method previously reported for preparing OA-capped ZnSe NPs.[47] The P3OT was dissolved in chloroform (concentration of 20 g l^{-1}). The mixture was then ultrasonicated for 2 hours at room temperature. The solution was then apportioned into bottles of 10 ml each to which the synthesized OA-capped CdSe NPs were added. Three different nanocomposites were prepared corresponding to the NPs concentrations, these are the pure polymer (0 wt%), the 40 wt% and 80 wt% respectively. The as-prepared solutions were ultrasonicated for 3 hours at room temperature.

The substrates were cleaned ultrasonically in distilled water, acetone, ethanol and distilled water sequentially for 15 min. These substrates were dried under a nitrogen gas stream. For the active layer deposition, we used the WS-400BZ-6NPP spin-coater from Laurell at 3000 rpm for 30 s. The last step was depositing a thin film (100 nm thick) of aluminum by using Vinci Technologies TDK-Lambda vacuum evaporator at a background pressure of $\approx 10^{-6}$ Pa. Fig. 1 illustrates the synthesis procedure of the P3OT:wt% OA-capped CdSe hybrid solution.

The morphologies and sizes of the OA-capped CdSe NPs were investigated using Tecnai G220 transmission electron microscope (TEM), atomic force microscope (AFM) and a JEOL JSM-6360 scanning electron microscope (SEM).

The structures of the NPs were investigated by X-ray diffraction using the Bruker D4 diffractometer. The Cu-K_α radiation ($\lambda = 1.5418$ Å) and Bragg–Brentano setup were used during the measurement of the XRD patterns. The dielectric properties were measured by an Agilent 4294A impedance analyzer in the frequency range 10 to 10^7 Hz. All the measurements were performed at ambient conditions of pressure and temperature.

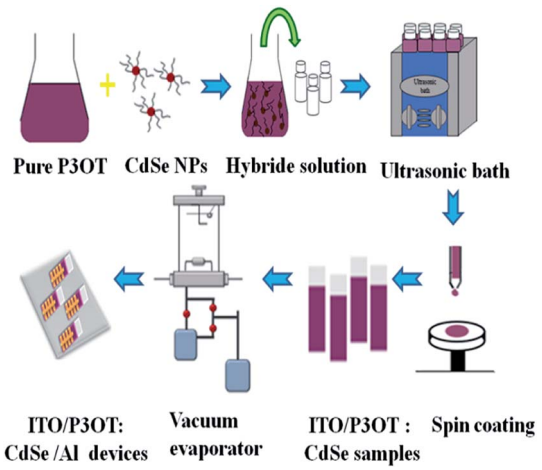

Fig. 1 Experimental procedure of the synthesis of P3OT:wt% OA-capped CdSe hybrid solution.

Results and discussion

Fig. 2(a) shows the XRD pattern of the OA-capped CdSe NPs in the range 20–80° 2θ. We observed five main broad diffraction peaks, of cubic zinc blend CdSe located at 25.7°, 42.3° 49.8°, 68.2° and 77.8° corresponding to the favorite orientations (111), (220), (311), (133) and (224) respectively. On the other hand, the shoulder peak near the (111) peak of our material may be indexed as (100) and attributed to the presence of uncapped CdSe nanoparticles of hexagonal (Wurtzite) structure.[48,49] We determine the average grain size by Scherrer's formula.[50]

$$D_{SC} = \frac{0.9 \times \lambda}{\beta \times \cos\theta} \quad (1)$$

where θ is the diffraction angle, λ is the wavelength of the X-ray and β is the full width at half maximum of the diffraction peak which may be expressed as:

$$\beta = (\beta_m{}^2 - \beta_i{}^2)^{1/2} \quad (2)$$

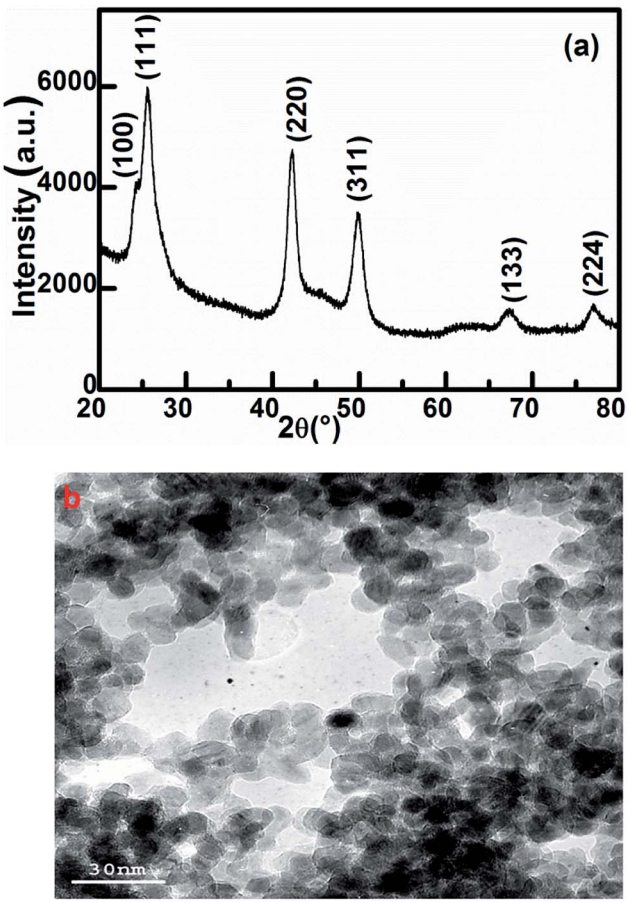

Fig. 2 (a) XRD patterns of the OA-capped CdSe NPs. (b) TEM image of the OA-capped CdSe NPs.

Open Access Article. Published on 22 December 2020. Downloaded on 1/15/2026 2:18:28 PM.
This article is licensed under a Creative Commons Attribution-NonCommercial 3.0 Unported Licence.

where β_i^2 is the Full Width at Half Maximum (FWHM) of standard silicon sample and β_m^2 is the experimental FWHM. The average grain size of OA-capped CdSe NPs is 8 nm.

Fig. 2(b) shows the CdSe NPs under TEM. The average diameter of the CdSe NPs is found equal to 8 nm in agreement with that obtained from the XRD measurements.

The P3OT:wt% OA-capped CdSe NPs thin films were investigated by SEM as shown in Fig. 3(a–c). The scanning electron micrographs show that the polymeric films are composed of grains stacked on the top of each other. The density of these grains varies from one region to another. The presence of these grains is believed to induce charge accumulation.[51] The morphology of the compound polymer is mainly formed by a small grains of lengths varying between 15 nm and 25 nm. This also involves the formation of a hierarchical network of pores as observed under the atomic force microscopy measurements.

The morphology of the deposited P3OT:wt% OA-capped CdSe NPs thin films, obtained using AFM, is shown in Fig. 4(a–c). By comparing the AFM images of the three concentrations prepared in this work, common features were identified. These features are attributed to the preparation condition rather than the NPs concentration in the thin films deposited. The distribution of the NPs obviously changes with the NPs concentration. The nanocomposite films do not cover the substrates totally. This might be attributed to the drying condition of the solution after the deposition process.[52,53] The fast drying of the chloroforme solvent is believed to influence the ordering of the P3OT polymer chains resulting in the features observed in the micro-images.[54] Similar topography features were observed in other types of polymers.[55,56] With regards to the deposition technique used, it is worth mentioning that J. Abad *et al.* investigated the effect of the deposition technique and found that the spin-coating technique yields a more homogeneous depositions than does the drop-casting technique.[57] We have shown that the OA-capped CdSe NPs affect the polymer chain entanglement and maximizes the interface of the P3OT/OA-capped CdSe heterojunction.[58] In contrast, the samples containing 40 wt% and 80 wt% of OA-capped CdSe show a decrease in the pore size and height. In the case of the polyvinylcarbazole : ZnSe NPs,

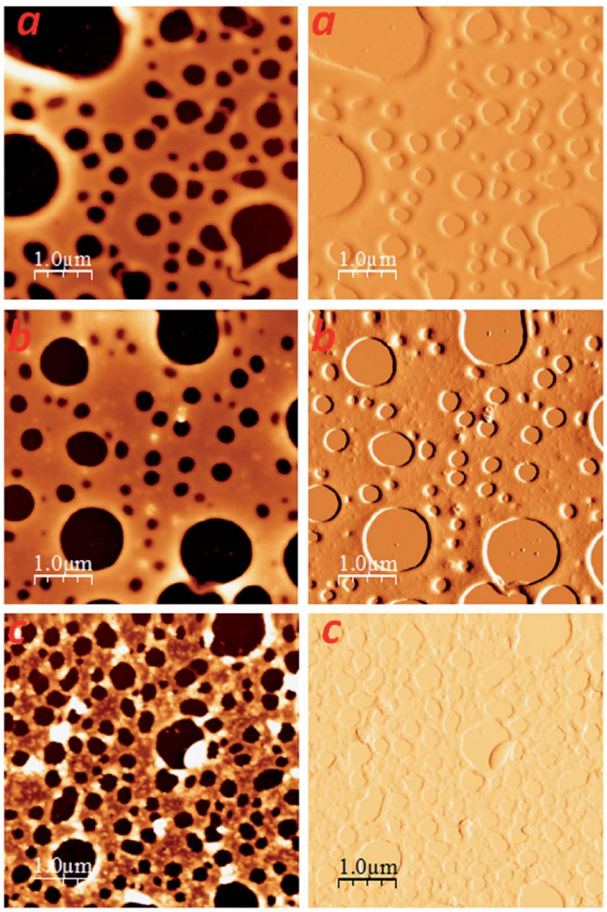

Fig. 4 Morphology of the deposited films of P3OT:wt% OA-capped CdSe NPs (a) wt 0% (b) wt 40% and (c) wt 80%.

increasing the NPs concentration in the polymer matrix was found to affect the topography of the films such that the pores network disappears almost completely at higher concentrations of the NPs. Such effect was attributed to the diffusion of the NPs into the polymer network. These NPs may affect the formation of the polymer percolating network.[59–61] As observed in the micrographs, the OA-capped CdSe NPs are well dispersed in the polymer matrix. This results in the augmentation of the

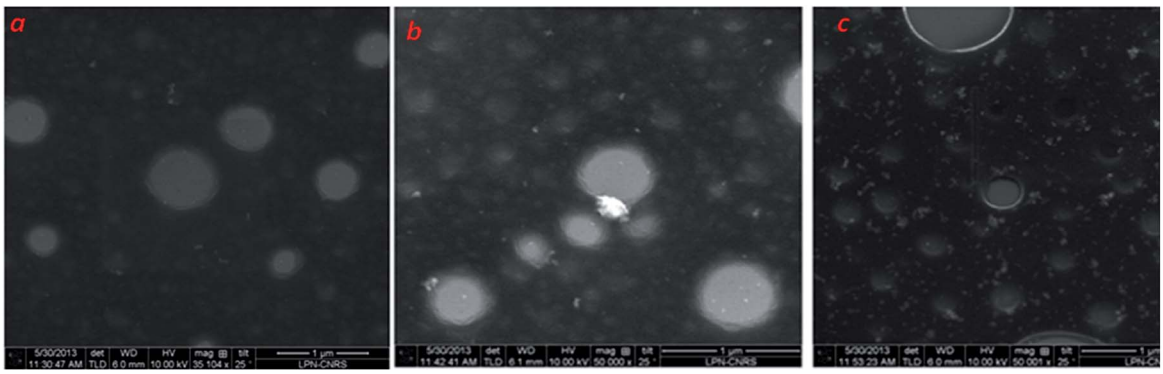

Fig. 3 SEM images of P3OT:wt% OA-capped CdSe NPs (a) pure (b) 40% wt (c) 80% hybrid thin films.

Open Access Article. Published on 22 December 2020. Downloaded on 1/15/2026 2:18:28 PM.
This article is licensed under a Creative Commons Attribution-NonCommercial 3.0 Unported Licence.

polymer/NPs interface leading to an increase in the probability of the exciton dissociation. The average roughness of the films varies from 12.79 nm to 22.27 nm. The roughness varies in an increasing way with concentration.

The increase of roughness enhances the oxygen adsorption process at the crystallites surfaces which act as electron traps. The topography evolution is found directly dependent on the concentration of the OA-capped CdSe NPs (Fig. 4(b and c)). The homogeneous dispersion of the NPs in addition to the pores network plays a major role in facilitating conduction paths of low resistance inducing an inter-chain charge transfer which leads to a gradual increase of conductivity of the P3OT:wt% OA-capped CdSe hybrid thin films.[62]

The electrical conductivity of the P3OT:wt% OA-capped CdSe thin films in the frequency range 10 to 10^6 Hz is shown in Fig. 5. Poor conductivity and insignificant dependence of its value on frequency are observed in the frequency range 50 to 10^4 Hz. At frequencies higher than 10^4 Hz significant increase of conductivity is observed. In this region, conductivity can be described by the power law:[63,64]

$$\sigma(\omega) = \sigma_d + A\omega^s \tag{3}$$

where A is a constant, σ_{dc} is the electrical conductivity, ω is the angular frequency and the exponent s (which depends on binding energy) is the slope of the plot in the frequency dependent region $0 \leq s \leq 1$.[65] Such behavior can be explained by the Maxwell–Wegner two-layer model suggesting that the layers are made of well conducting grains surrounded by poorly conducting grain boundaries that are more active at lower frequencies. The electrical conductivity occurs by hopping of charge carriers between defect states in the band gap and the AC conductivity corresponding to a jump of localized charge carriers in defect sites separated by potential barriers and therefore it is hopping type conduction.[66] The conductivity curve shows an increase in value with the increase in the concentration of the oleic acid capped CdSe NPs. This may be attributed to the surface morphology and a homogeneous dispersion of the OA-capped CdSe NPs in the P3OT matrix which improves charge conduction at the polymer : NPs interface.[67] The complex impedance Z is given by the following equation:[68]

$$Z = Z' - jZ'' \tag{4}$$

where Z' and Z'' are the real and imaginary components of impedance respectively. Fig. 6 shows the dependence of Z' on frequency for the three concentrations investigated. Z decreases slowly with the increase of frequency up to 5×10^3 Hz. A rapid decrease of the real component of impedance occurs at frequencies in the range 10^4 to 10^5 Hz. A third region may be identified at frequencies higher than 10^5 Hz where insignificant dependence of impedance on frequency occurs. In the first two regions identified, Z' decreases with the increase of NPs concentration. This is attributed to the homogeneous distribution of NPs and the decrease of NPs clustering in the polymer matrix. The acute decay of Z' at frequencies higher than 10^5 Hz may be attributed to the space-charge regions resulting from the decline of the charge barrier. The Z' variation with frequency complies with the structural information obtained.

The imaginary component of impedance (Z'') of and the P3OT:wt% OA-capped CdSe hybrid thin films as a function of frequency. The variation of the imaginary part of impedance Z'' with the frequency at the three concentrations investigated is shown in Fig. 7. A peak-like behavior of the Z'' at two frequency values is observed for the three polymers : NPs films prepared. The first peak at low frequency value is associated with the effects of the grains boundaries while the second peak at 5×10^4 Hz is attributed to the relaxation of these effects. Z'' was found to generally decrease with the increase of NPs concentration. The impedance results emphasize that the inclusion and dispersion of the OA-capped CdSe NPs have a profound effect on the impedance characteristics of the samples. This behavior may be associated with two phenomena and affect the impedance spectroscopy results. The first one, is the P3OT/OA-capped CdSe interface contact and the second one is medium and severe clusters formation (*i.e.* polymer clusters, NPs clusters and complex clusters[69]) related to the overall decrease of

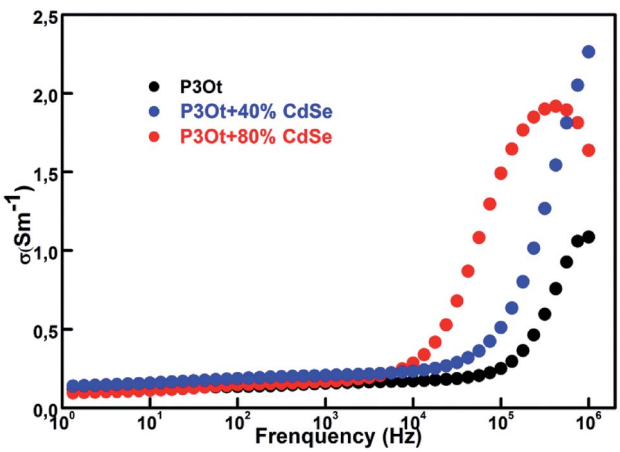

Fig. 5 Electrical conductivity of P3OT:wt% OA-capped CdSe hybrid thin film as a function of frequency.

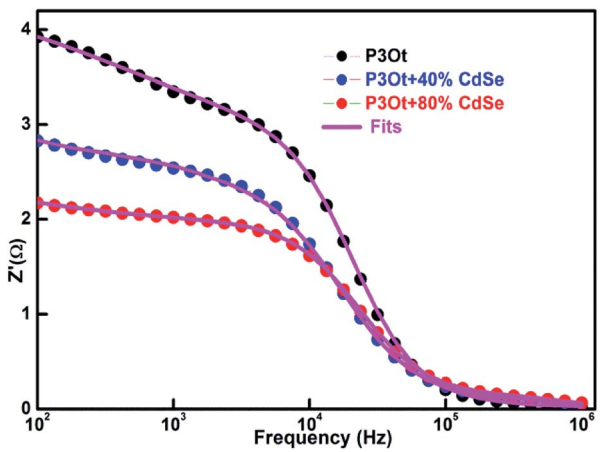

Fig. 6 Real component of impedance of P3OT:wt% OA-capped CdSe hybrid thin film as a function of frequency.

Open Access Article. Published on 22 December 2020. Downloaded on 1/15/2026 2:18:28 PM.
This article is licensed under a Creative Commons Attribution-NonCommercial 3.0 Unported Licence.

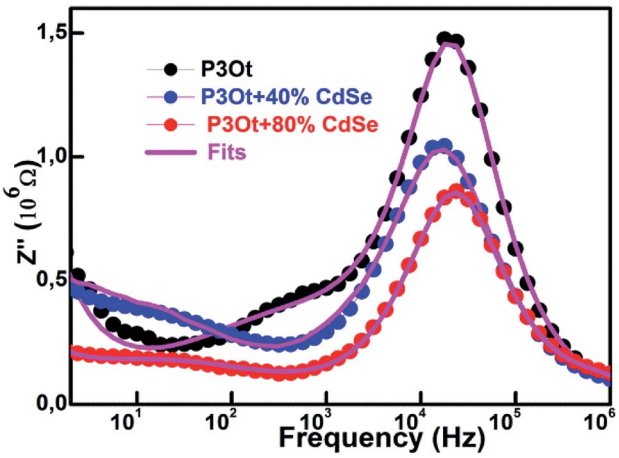

Fig. 7 Imaginary component of impedance of P3OT:wt% OA-capped CdSe NPs as a function of frequency.

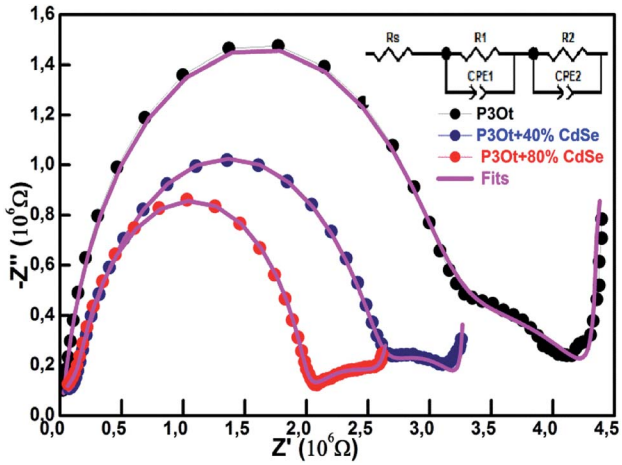

Fig. 9 Nyquist diagram of P3OT:wt% OA-capped CdSe NPs hybrid thin film. The inset shows the equivalent circuit.

impedance. We would also point out the weak peaks located at the grain resistance region. In the frequency range above 10^7 Hz the merging of Z'' may easily be noticed indicating a decrease in the space charge polarization.[70]

In order to determine the relaxation time value, we plot the curves of Z' and Z'' according to the frequency. The frequency f_{max}, at which the impedance Z'' takes its maximum value, corresponds to the inflection point abscissa to the curve of variations of Z' as a function of the frequency.[71]

In Fig. 8 we got two inflection points, thus two frequency maxima at 360 Hz and 4.5×10^4 Hz. The relaxation time is calculated from these values using the following equation:[72]

$$\tau = \frac{1}{2\pi f_{max}} \tag{5}$$

Fig. 9 is the Nyquist plots of the P3OT:wt% OA-capped CdSe NPs hybrid thin films. Two semicircles of different sizes and a linear segment are observed in all the specimens investigated indicating that the key sources of impedance are the same and independent of the OA-capped CdSe NPs. Nevertheless, the semicircle feature which emphasizes the two components/sources of impedance (namely, the double-layer effect at the grain boundaries of the polymer/NPs interface and the charge transfer through the composite material) are found to vary with the concentration of NPs inside the specimen. The decrease of the semicircles sizes with the increase of NPs is attributed to the enhancement of the charge carrier's mobility throughout these charges transferring centers.

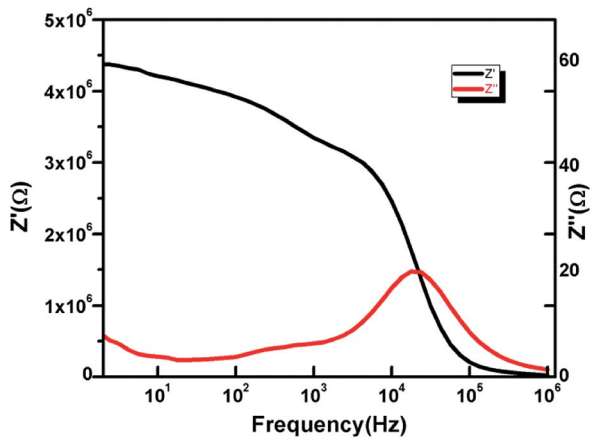

Fig. 8 Variation of Z' and Z'' of P3OT:wt% OA-capped CdSe NPs hybrid thin film with frequency.

The equivalent circuit is shown in the inset of Fig. 9. Our simulations of the Nyquist plots agree with the measurements and the equivalent circuit was found to reproduce the experimental plots by adjusting the controlling parameters.

The equivalent circuit is composed of two R-CPE (constant phase element) components in parallel with a third resistance R_s has conventionally known Warburg impedance. Warburg impedance is due to lack/depletion of species that otherwise may undergo certain reactions (oxidation/reduction reactions). In the present work, this component is attributed to presence of conductivity zones inside the material associated with the ITO/active layer interface.[73,74]

The CPE is determined using the following relation:

$$Z^*(\omega) = \frac{R}{1 + \left(\frac{j\omega}{\omega_0}\right)^{1-n}} \tag{6}$$

when $n \to 0$ it results in the classical Debye's formulae. Thus, the total impedance of the structure can be written as:

$$Z^* = \sum_{i=1}^{n=2} \frac{[A_i(j\omega)^{\alpha_i}]^{-1} R_i}{[A_i(j\omega)^{\alpha_i}]^{-1} + R_i} + R_s = Z' - jZ'' \tag{7}$$

where Z' and Z'' are given by the following equations:

$$Z' = \sum_{i=1}^{n=2} \frac{R_i\left(1 + R_i A_i \omega^{\alpha_i} \cos\left(\frac{\pi}{2}\alpha_i\right)\right)}{\left(R_i A_i \omega^{\alpha_i} \sin\left(\frac{\pi}{2}\alpha_i\right)\right)^2 + \left(1 + R_i A_i \omega^{\alpha_i} \cos\left(\frac{\pi}{2}\alpha_i\right)\right)^2} + R_s \tag{8}$$

Open Access Article. Published on 22 December 2020. Downloaded on 1/15/2026 2:18:28 PM.
This article is licensed under a Creative Commons Attribution-NonCommercial 3.0 Unported Licence.

Table 1 R_s, R_1 and R_2 of P3OT:wt% OA-capped CdSe hybrid thin films

Sample	R_s (Ω)	R_1 (Ω)	R_2 (Ω)
P3OT	1523	2.7488×10^6	1.6649×10^3
P3OT:40% CdSe	1145	2.1144×10^6	7.6823×10^2
P3OT:80% CdSe	940	7.7361×10^4	1.953×10^2

$$Z'' = \sum_{i=1}^{n=2} \frac{R_i^2 A_i \omega^{\alpha_i} \sin\left(\frac{\pi}{2}\alpha_i\right)}{\left(R_i A_i \omega^{\alpha_i} \sin\left(\frac{\pi}{2}\alpha_i\right)\right)^2 + \left(1 + R_i A_i \omega^{\alpha_i} \cos\left(\frac{\pi}{2}\alpha_i\right)\right)^2} \quad (9)$$

The values of constant phase element A_i and resistances R_i for various OA-capped CdSe NPs concentration are listed in Table 1. The data presented a sharp decrease of three resistances when OA-capped CdSe NPs concentration increases. This behavior is explained by different contacts on each side of the pellet and different charge conduction zones. A_s resistance decreases conductivity increases accordingly.

The Frequency dependence of real permittivity ε' at different OA-capped CdSe NPs concentration is shown in Fig. 10. We noticed that permittivity increases with the concentration of the NPs and this behavior become more significant at low frequency values. At frequencies, less than 10^4 Hz the real value of permittivity increases with the concentration of NPs indicating that charge carriers are influenced by dipolar and interfacial polarization. This trend, is explained by the Maxwell–Wagner double layer model designed for inhomogeneous structures. At higher frequencies, ionic and electronic polarization contribute to the dielectric constant and they are frequency independent.[75,76] Thus, the effect of OA-capped CdSe NPs concentration on dielectric constant is negligible. This could be attributed to the reverse electron motion as the frequency increases leading to reduced polarization.

Fig. 11 exhibits the variation of imaginary permittivity as a function of frequency at different OA-capped CdSe NPs concentrations. At frequencies less that 10^3 Hz the imaginary value of permittivity is frequency-on frequency and OA-capped CdSe NPs, contrarily to the strong dependence behavior on frequency seen from the same spectra. Fig. 10 exhibits the variation of imaginary permittivity as a function of frequency at different capon. We note that for frequency ($f < 10^3$ Hz) the imaginary permittivity dependence on frequency and OA-capped CdSe NPs concentration. The plots clearly show that curves decreasing as the frequency rises. As the frequency continues to rise, the dielectric constant also continues to lessen. This behavior is explained by the pattern of grain and grain seal or the grain boundaries possess high resistance, so the electrons gather and generate polarization at the boundaries. Thereafter, we notice a rapid decrease of the dielectric constant until independent of frequency.

Fig. 12 shows the variation of the dielectric loss (tan δ) with frequency at different concentrations of the CdSe NPs. Three regions may be observed. Low-frequency region (50 to 10^3 Hz) we notice high loss for the different concentration of CdSe NPs

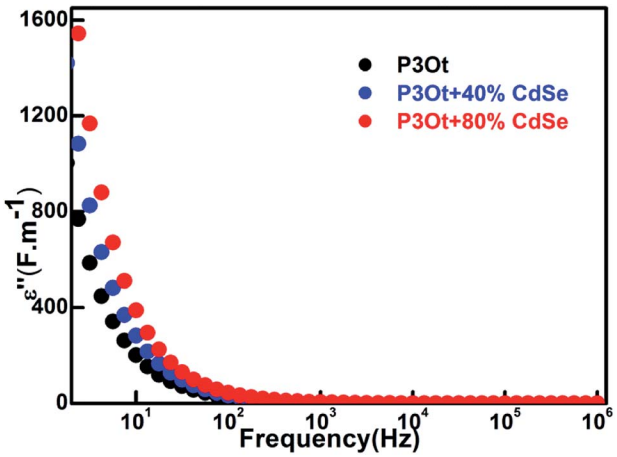

Fig. 11 Imaginary part of dielectric constant of P3OT:wt% OA-capped CdSe hybrid thin films as a function of frequency.

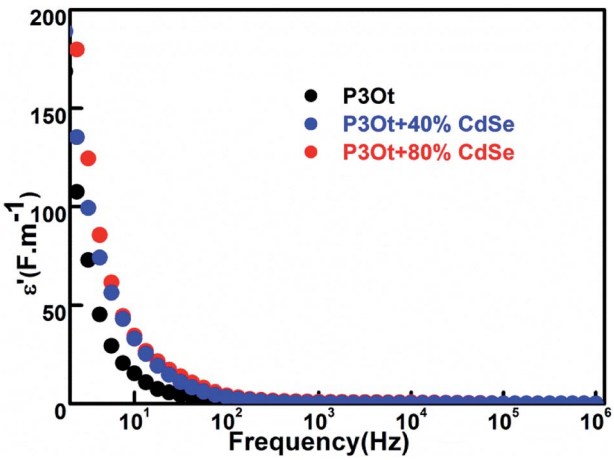

Fig. 10 Real part of dielectric constant of P3OT:wt% OA-capped CdSe hybrid thin films as a function of frequency.

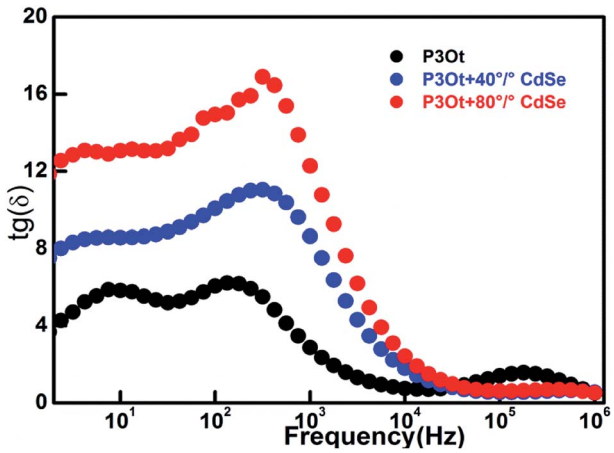

Fig. 12 Tangent loss of P3OT:wt% OA-capped CdSe hybrid thin films as a function of frequency.

Open Access Article. Published on 22 December 2020. Downloaded on 1/15/2026 2:18:28 PM.
This article is licensed under a Creative Commons Attribution-NonCommercial 3.0 Unported Licence.

then the tan δ decreases as of frequency, followed by a new growth between 5×10^3 Hz and 5×10^4 Hz. The elevated resistance of grain boundaries at low frequencies results in electrons requiring high energy which justifies the high values of dielectric loss at that region according to Koop's theory.[77] The growth in the second region can be explained by the piling up of the electrons at the grain boundaries through a hopping mechanism. There is a reduction of dielectric loss for the higher frequencies and continues to gradually decrease tending towards zero irrespective to OA-capped CdSe NPs concentration. This coalescence is due to the poor energy loss during the exchange of load carriers.

Enhancing the dielectric parameters of conjugated polymers is an attractive prospect for optoelectronic and microelectronic devices.[78,79] The evolution of the dielectric permeability of our samples as a function of frequency covers a large range of frequency (10 to 10^6), such a similar frequency range is showed by Talfah *et al.*[68] The value of P3OT dielectric constant is very high in comparison with of Aromatic polythiourea (ArPTU) and polyvinylidene fluoride.[80] At high frequency, the dipoles cannot follow the oscillation of the applied electric field and the dielectric constant become constant.[81] We notice that the contact resistance R_s decreasing when the concentration of NPs increases.[67] Generally, there is only one relaxation frequency in polymers, here in our materials, we found two relaxation frequency.[82]

Conclusion

Thin films of P3OT mixed with oleic acid-capped cadmium selenide NPs were synthesized and deposited successfully by a spin coating method to form a hybrid heterojunction for dielectric applications. The AC electrical conductivity study revealed a strong dependence of conductivity as a function of frequency and concentration of the CdSe NPs. The impedance spectroscopy measurements showed that the charge mobility increases with the increase of the NPs. Two relaxation frequencies were also observed. Agreement between the experimental curves and the simulation data was obtained. We have determined the equivalent circuit for our composite. The circuit is formed by a series of two *R*-CPE in parallel combination and a third resistance conventionally known as Warburg impedance. Permittivity was found to increase with the concentration of the NPs. The electrical behavior of the dielectric material was associated with the two region effect at the grain boundaries of the polymer/NPs interface and the grain of the composite material.

Conflicts of interest

There are no conflicts to declare.

References

1 M. E. Hajlaoui, N. Hnainia, Z. Gouid, A. Benchaabane, M. A. Sanhoury and R. Chtourou, Optimization of hybrid P3HT:CdSe photovoltaic devices through surface ligand modification, *Mater. Sci. Semicond. Process.*, 2020, **109**, 104934.

2 E. Salim, S. R. Bobbara, A. Oraby and J. M. Nunzi, Copper oxide nanoparticle doped bulk-heterojunction photovoltaic devices, *Synth. Met.*, 2019, **252**, 21–28.

3 J. Satra, P. Mondal, U. K. Ghorui and B. Adhikary, *In situ* systematic metallic gold incorporation to optimize the photon conversion efficiency of $AgInS_2$ thin film semiconductor, *Sol. Energy Mater. Sol. Cells*, 2019, **195**, 24–33.

4 W. Ouyang, J. Chen, J. He and X. Fang, Improved Photoelectric Performance of UV Photodetector Based on ZnO Nanoparticle-Decorated BiOCl Nanosheet Arrays onto PDMS Substrate: The Heterojunction and $Ti_3C_2T_x$ MXene Conduction Layer, *Adv. Electron. Mater.*, 2020, **6**, 2000168.

5 J. Chen, W. Ouyang, W. Yang, J. H. He and X. Fang, Recent Progress of Heterojunction Ultraviolet Photodetectors: Materials, Integrations, and Applications, *Adv. Funct. Mater.*, 2020, **30**, 1909909.

6 K. M. A. Saron, M. R. Hashim, M. Ibrahim, M. Yahyaouiad and N. K. Allam, Temperature-dependent transport properties of CVD-fabricated n-GaN nanorods/p-Si heterojunction devices, *RSC Adv.*, 2020, **10**, 33526–33533.

7 N. Tessler, V. Medvedev, M. Kazes, S. H. Kan and U. Banin, Efficient near-infrared polymer nanocrystal light-emitting diodes, *Science*, 2002, **295**, 1506–1508.

8 A. Benchaabane, Z. Ben Hamed, A. Telfah, M. A. Sanhoury, F. Kouki, K. Zellama and H. Bouchriha, Effect of OA-ZnSe nanoparticles incorporation on the performance of PVK organic photovoltaic cells, *Mater. Sci. Semicond. Process.*, 2017, **64**, 115–123.

9 A. Benchaabane, J. Belhadi, Z. Ben Hamed, M. Lejeune, A. Lahmar, M. A. Sanhoury, F. Kouki, K. Zellama, A. Zeinert and H. Bouchriha, Effect of CdSe incorporation on the performance of P3OT organic photovoltaic cells, *Mater. Sci. Semicond. Process.*, 2016, **41**, 343–349.

10 P. Reiss, E. Couderc, J. D. Girolamo and A. Porn, Conjugated polymers/semiconductor nanocrystals hybrid materials preparation, electrical transport properties and applications, *Nanoscale*, 2011, **3**, 446–489.

11 J. Salfi, U. Philipose, C. F. d. Sousa, S. Aouba and H. E. Ruda, Electrical properties of ohmic contacts to ZnSe nanowires and their application to nanowire-based photodetection, *Appl. Phys. Lett.*, 2006, **89**, 261112.

12 M. Belhaj, C. Dridi, R. Yatskiv and J. Grym, The improvement of UV photodetection based on polymer/ZnO nanorod heterojunctions, *Org. Electron.*, 2020, **77**, 105545.

13 M. K. Mohanapriya, K. Deshmukh, K. Chidambaram, M. B. Ahamed, K. K. Sadasivuni, D. Ponnamma, M. A. A. AlMaadeed, R. R. Deshmukh and S. K. K. Pasha, Polyvinyl alcohol (PVA)/polystyrene sulfonic acid (PSSA)/carbon black nanocomposite for flexible energy storage device applications, *J. Mater. Sci.: Mater. Electron.*, 2017, **28**, 6099–6111.

14 X. S. Fang, C. H. Ye, L. D. Zhang and T. Xie, Twinning-Mediated Growth of Al_2O_3 Nanobelts and Their Enhanced Dielectric Responses, *Adv. Mater.*, 2005, **17**, 1661–1665.

Open Access Article. Published on 22 December 2020. Downloaded on 1/15/2026 2:18:28 PM.
This article is licensed under a Creative Commons Attribution-NonCommercial 3.0 Unported Licence.

15 J. H. Son, J. H. Kim, D. H. Park, W. K. Choi, F. Li, J. H. Ham and T. W. Kim, Nonvolatile flexible organic bistable devices fabricated utilizing CdSe/ZnS nanoparticles embedded in a conducting poly-*N*-vinylcarbazole polymer layer, *Nanotechnology*, 2008, **19**, 055204.

16 W. L. Leong, P. S. Lee, S. G. Mhaisklkar, T. P. Chen and A. Dodablapur, Charging phenomena in pentacene- gold nanoparticle memory device, *Appl. Phys. Lett.*, 2007, **90**, 042906.

17 W. Ouyang, F. Teng and X. Fang, High Performance BiOCl Nanosheets/TiO_2 Nanotube Arrays Heterojunction UV Photodetector: The Influences of Self-Induced Inner Electric Fields in the BiOCl Nanosheets, *Adv. Funct. Mater.*, 2018, **28**, 1707178.

18 F. Li, Z. Qiang, S. Chen, J. Wei, T. Li and D. Zhangd, Synthesis of CdS-loaded $(CuC_{10}H_{26}N_6)_3(PW_{12}O_{40})_2$ for enhanced photocatalytic degradation of tetracycline under simulated solar light irradiation, *RSC Adv.*, 2020, **10**, 37072–37079.

19 E. J. Bailey and K. I. Winey, Dynamics of Polymer Segments, Polymer Chains, and Nanoparticles in Polymer Nanocomposite Melts: A Review, *Prog. Polym. Sci.*, 2020, **105**, 101242.

20 C. Zhang, P. L. Yu, Y. Li and J. C. Li, Polymer/TiO_2 nanoparticles interfacial effects on resistive switching under mechanical strain, *Org. Electron.*, 2020, **77**, 105528.

21 X. Zhu, B. Guo, F. Jin, T. Zhai, Y. Wang, G. Li, J. Zhang, Z. Wei, S. Duhm, X. Guo, M. Zhang and Y. Li, Surface modification of ZnO electron transport layers with glycine for efficient inverted non-fullerene polymer solar cells, *Org. Electron.*, 2019, **70**, 25–31.

22 M. M. Alam, M. Z. B. Mukhlish, A. Tazrin, N. A. Jui, A. M. Asiri, M. M. Rahman, M. A. Islama and M. T. Uddin, A novel highly selective electrochemical chlorobenzene sensor based on ternary oxide RuO_2/ZnO/TiO_2 nanocomposites, *RSC Adv.*, 2020, **10**, 32532–32547.

23 D. I. Son, J. H. Kim, D. H. Park, W. K. Choi, F. Li, J. H. Ham and T. W. Kim, Nonvolatile flexible organic bistable devices fabricated utilizing CdSe/ZnS nanoparticles embedded in a conducting poly-*N*-vinylcarbazole polymer layer, *Nanotechnology*, 2008, **19**, 055204.

24 L. Zhao, L. Hu and X. Fang, Growth and Device Application of CdSe Nanostructures, *Adv. Funct. Mater.*, 2012, **22**, 1551–1566.

25 W. L. Leong, P. S. Lee, S. G. Mhaisklkar, T. P. Chen and A. Dodablapur, Charging phenomena in pentacene-gold nanoparticle memory device, *Appl. Phys. Lett.*, 2007, **90**, 042906.

26 B. Cho, T. W. Kim, M. Choe, G. Wang, S. Song and T. Lee, Unipolar nonvolatile memory devices with composites of poly(9-vinylcarbazole) and titanium dioxide nanoparticles, *Org. Electron.*, 2009, **10**, 473–477.

27 M. Vilkman, K. Solehmainen, A. Laiho, H. G. O. Sandberg and O. Ikkala, Negative differential resistance in polymeric memory devices containing disordered block copolymers with semiconducting block, *Org. Electron.*, 2009, **10**, 1478–1482.

28 V. S. Reddy, S. Karak, S. K. Rayand and A. Dhar, Carrier transport mechanism in aluminum nanoparticle embedded AlQ_3 structures for organic bistable memory devices, *Org. Electron.*, 2009, **10**, 138–144.

29 A. Benchaabane, Z. B. Hamed, F. Kouki, A. Zeinert and H. Bouchriha, Photogeneration process in bulk heterojunction solar cell based on quaterthiophene and CdS nanoparticles, *Appl. Phys. A*, 2015, **120**, 1149–1157.

30 A. Benchaabane, Z. Ben Hamed, A. Telfah, M. A. Sanhoury, F. Kouki, K. Zellama and H. Bouchriha, Effect of OA-ZnSe nanoparticles incorporation on the performance of PVK organic photovoltaic cells, *Mater. Sci. Semicond. Process.*, 2017, **64**, 115–123.

31 D. S. Ginger and N. C. Greenham, Charge injection and transport in films of CdSe nanocrystals, *J. Appl. Phys.*, 2000, **87**, 1361–1368.

32 K. F. Jeltsch, M. Schadel, J.-B. Bonekamp, *et al.*, Efficiency enhanced hybrid solar cells using a blend of quantum dots and nanorods, *Adv. Funct. Mater.*, 2012, **22**, 397–404.

33 K. Kumari, S. Chand, V. D. Vankar and V. Kumar, Enhancement in hole current density on polarization in poly(3-hexylthiophene): cadmium selenide quantum dot nanocomposite thin films, *Appl. Phys. Lett.*, 2009, **94**, 213503.

34 S. L. Mousavi, F. J. Sheini, M. Sabaeian and R. Yousef, Enhanced solar cell performance of P3HT:PCBM by SnS nanoparticles, *Sol. Energy*, 2020, **199**, 872–884.

35 P. Mahajan, A. Singh and S. Arya, Improved performance of solution processed organic solar cells with an additive layer of sol-gel synthesized ZnO/CuO core/shell nanoparticles, *J. Alloys Compd.*, 2020, **814**, 152292.

36 Y. J. Park, K. S. Lee, G. H. Lim, H. W. Seo, S. W. Kim, M. Kim, Y. Yi, H. S. Lee and D. I. Son, Role of CdSe and CdSe@ZnS quantum dots interlayers conjugated in inverted polymer solar cells, *Org. Electron.*, 2020, **82**, 105707.

37 W. A. Zoubi, M. P. Kamil, S. Fatimah, N. Nashrah and Y. G. Ko, Recent advances in hybrid organic–inorganic materials with spatial architecture for state-of-the-art applications, *Prog. Mater. Sci.*, 2020, **112**, 100663.

38 M. Nabil, S. A. Mohamed, K. Easawi, S. S. A. Obayya, S. Negm, H. Talaat and M. K. El-Mansy, Surface modification of CdSe nanocrystals: application to polymer solar cell, *Curr. Appl. Phys.*, 2020, **20**, 470–476.

39 M. J. Greaney, S. Das, D. H. Webber, S. E. Bradforth and R. L. Brutchey, Improving Open Circuit Potential in Hybrid P3HT:CdSe Bulk Heterojunction Solar Cells *via* Colloidal *tert*-Butylthiol Ligand Exchange, *J. Am. Chem. Soc.*, 2012, **6**, 4222–4230.

40 Y. Zhou, F. S. Riehle, Y. Yuan, H. F. Schleiermacher, M. Niggeman, G. A. Urban and M. Kruger, Improved efficiency of hybrid solar cells based on non-ligand-exchanged CdSe quantum dots and poly(3-hexylthiophene), *Appl. Phys. Lett.*, 2010, **96**, 013304.

41 C. Bullen and P. Mulvaney, The Effects of Chemisorption on the Luminescence of CdSe Quantum Dots, *Langmuir*, 2006, **22**, 3007–3013.

42 J. Chen, J. L. Song, X. W. Sun, W. Q. Deng, C. Y. Jiang, W. Lei, J. H. Huang and R. S. Liu, An oleic acid-capped CdSe

Open Access Article. Published on 22 December 2020. Downloaded on 1/15/2026 2:18:28 PM. This article is licensed under a Creative Commons Attribution-NonCommercial 3.0 Unported Licence.

quantum-dot sensitized solar cell, *Appl. Phys. Lett.*, 2009, **94**, 153115.

43 P. K. Khanna, K. S. Rao, K. R. Patil, V. N. Singh and B. R. Mehta, One-pot synthesis of oleic acid-capped cadmium chalcogenides (CdE:E5 Se,Te) nano-crystals, *J. Nanopart. Res.*, 2010, **12**, 101–109.

44 N. K. Shrestha, S. J. Yoon, C. Bathula, H. Opoku and Y.-Y. Noh, Hole-induced polymerized interfacial film of polythiophene as co-sensitizer and back-electron injection barrier layer in dye-sensitized TiO_2 nanotube array, *J. Alloys Compd.*, 2019, **781**, 589–594.

45 E. G. M. Morales-Espinoza, A. Ruiu, B. X. Valderrama-García, J. Duhamel and E. Rivera, Design, characterization, optical and photophysical properties of novel thiophene monomers and polymers containing pyrene moieties linked *via* rigid and flexible spacers, *Synth. Met.*, 2019, **248**, 102–109.

46 S. Bhattacharyya and A. Patra, Interactions of π-conjugated polymers with inorganic nanocrystals, *J. Photochem. Photobiol., C*, 2014, **20**, 51–70.

47 K. S. Rao, N. Singh, K. Gurunathan, R. Marimuthu, N. R. Munirathanam, T. L. Prakash and P. K. Khanna, Nearly mono-disperse quantum dots of ZnSe: synthesis and characterization, *Synth. React. Inorg., Met.-Org., Nano-Met. Chem.*, 2007, **37**, 497.

48 V. Tzitzios, V. Georgakilas, I. Zafiropoulou, N. Boukos, G. Basina, D. Niarchos and D. Petridis, A General Chemical Route for the Synthesis of Capped Nanocrystalline Materials, *J. Nanosci. Nanotechnol.*, 2007, **8**, 1–6.

49 X. Xia, Z. Liu, G. Du, Y. Li and M. Ma, Wurtzite, zinc-blende CdSe based core/shell semiconductor nanocrystals: structure, morphology and photoluminescence, *J. Lumin.*, 2010, **130**, 1285–1291.

50 *Théorie et Technique de la radiocristallographie*, ed. A. Guinier and X. Dunod, 3rd edn, 1964, p. 462.

51 L. Shi, Y. Yin, L. C. Zhang, S. Wang, M. Sillanpaa and H. Sun, Design and engineering heterojunctions for the photoelectrochemical monitoring of environmental pollutants: a rev., *Appl. Catal., B*, 2019, **248**, 405–422.

52 W. Takashima, S. S. Pandey, T. Endo, M. Rikukawa, N. Tanigaki, Y. Yoshida, K. Yase and K. Kaneto, Photocarrier transports related to the morphology of regioregular poly(3-hexylthiophene) films, *Thin Solid Films*, 2001, **393**, 334–342.

53 M. Skompska, Hybrid conjugated polymer/semiconductor photovoltaic cells, *Synth. Met.*, 2010, **160**, 1–15.

54 L. Xu, H. Zhang, Y. Lu, L. An and T. Shi, The effects of solvent polarity on the crystallization behavior of thin π-conjugated polymer film in solvent mixtures investigated by grazing incident X-ray diffraction, *Polymer*, 2020, **190**, 122259.

55 R. Potai, A. Kamphan and R. Traiphol, On the formation of non-emissive and emissive aggregates of regioregular poly(3-octylthiophene) in different local environments, *Synth. Met.*, 2014, **187**, 136–144.

56 M. E. Nicho, C. H. García-Escobar, M. C. Arenas, P. Altuzar-Coello, R. Cruz-Silva and M. Güizado-Rodríguez, Influence of P3HT concentration on morphological, optical and electrical properties of P3HT/PS and P3HT/PMMA binary blends, *Mater. Sci. Eng., B*, 2011, **176**, 1393–1400.

57 J. Abad, B. Pérez-García, A. Urbina, J. Colchero and E. Palacios-Lidón, Layered self-organized structures on poly(3-octylthiophene) thin films studied by scanning probe microscopy, *Eur. Polym. J.*, 2008, **44**, 2506–2515.

58 A. Benchaabane, Z. Ben Hamed, F. Kouki, A. Zeinert and H. Bouchriha, Photogeneration process in bulk heterojunction solar cell based on quaterthiophene and CdS nanoparticles, *Appl. Phys. A*, 2015, **120**, 1149–1157.

59 A. Benchaabane, Z. Ben Hamed, F. Kouki, M. A. Sanhoury, K. Zellama, A. Zeinert and H. Bouchriha, Performances of effective medium model in interpreting optical properties of polyvinylcarbazole: ZnSe nanocomposites, *J. Appl. Phys.*, 2014, **115**, 134313.

60 M. Taghavimehr, M. Hossein, N. Famili and M. A. Shirsavar, Effect of nanoparticle network formation on electromagnetic properties and cell morphology of microcellular polymer nanocomposite foams, *Polym. Test.*, 2020, **86**, 106469.

61 A. Cingolani, D. Cuccato, G. Storti and M. Morbidelli, Control of Pore Structure in Polymeric Monoliths Prepared from Colloidal Dispersions, *Macromol. Mater. Eng.*, 2018, **303**, 1700417.

62 S. Biswas, D.-K. Kim, I.-W. Nam, M. Choi, J.-H. Bae and H. Kim, Highly conductive and thermally stable nanoparticle-conjugated polymer compounds through environmentally friendly *in situ* synthesis, *Prog. Org. Coat.*, 2020, **142**, 105606.

63 M. E. Hajlaoui, R. Dhahri, N. Hnainia, A. Benchaabane, E. Dhahri and K. Khirouni, Conductivity and giant permittivity study of $Zn_{0.5}Ni_{0.5}Fe_2O_4$ spinel ferrite as a function of frequency and temperature, *RSC Adv.*, 2019, **9**, 32395.

64 M. Atif and M. Nadeem, Sol–gel synthesis of nanocrystalline $Zn_{1-x}Ni_xFe_2O_4$ ceramics and its structural, magnetic and dielectric properties, *J. Sol-Gel Sci. Technol.*, 2014, **72**, 615–626.

65 S. Mollah, K. K. Som, K. Bose and B. K. Chaudri, ac conductivity in $Bi_4Sr_3Ca_3Cu_yO_x$ ($y = 0 - 5$) and $Bi_4Sr_3Ca_{3-z}Li_zCu_4O_x$ ($z = 0.1 - 1.0$) semiconducting oxide glasses, *J. Appl. Phys.*, 1993, **74**, 931.

66 H. Rahmouni, A. Benali, B. Cherif, E. Dhahri, M. Boukhobza, K. Khirouni and M. Sajieddine, Structural and electrical properties of $Zn_{1-x}Ni_xFe_2O_4$ ferrite, *Appl. Phys. B*, 2015, **466–467**, 31–37.

67 A. Benchaabane, Z. Ben Hamed, M. A. Sanhoury, F. Kouki, A. Zeinert and H. Bouchriha, Influence of nanocrystal concentration on the performance of hybrid P3HT:TBPO-capped CdSe nanocrystal solar cells, *Appl. Phys. A*, 2016, **122**, 60–70.

68 A. Telfah, M. M. Abdul, G. Jafar, I. Jum'h, M. J. A. Ahmad, J. Lambert and R. Hergenröder, Identification of relaxation processes in pure polyethylene oxide (PEO) films by the dielectric permittivity and electric modulus formalisms, *Polym. Adv. Technol.*, 2018, **29**, 1974–1987.

Open Access Article. Published on 22 December 2020. Downloaded on 1/15/2026 2:18:28 PM.
This article is licensed under a Creative Commons Attribution-NonCommercial 3.0 Unported Licence.

69 Z. BenHamed, N. Mastour, A. Benchaabane, F. Kouki, M. A. Sanhoury and H. Bouchriha, Franck–Condon analysis of fluorescence quenching in hybrid P3HT:wt% TBPO-capped CdSe quantum dot matrix, *J. Lumin.*, 2016, **170**, 30–36.

70 E. V. Ramana, S. V. Suryanarayana and T. B. Sankaram, Ac impedance studies of ferro electromagnetic $SrBi_{5-x}La_xTi_4FeO_{18}$ ceramics, *Mater. Res. Bull.*, 2006, **41**, 1077–1088.

71 M. E. Hajlaoui, R. Dhahri, N. Hnainia, A. Benchaabane, E. Dhahri and K. Khirouni, Dielectric spectroscopy study of the $Ni_{0.2}Zn_{0.8}Fe_2O_4$ spinel ferrite as a function of frequency and temperature, *Mater. Sci. Eng., B*, 2020, **262**, 114683.

72 K. Ashok, M. B. Suresh and P. Sarah, Electrical properties of Li and Nd doped $SrBi_4Ti_4O_{15}$ ceramics, *Int. J. Pure Appl. Res. Eng. Technol.*, 2013, **2**, 3299–3307.

73 V. S. Reddy, S. Das, S. K. Ray and A. Dhar, Studies on conduction mechanisms of pentacene based diodes using impedance spectroscopy, *J. Phys. D: Appl. Phys.*, 2007, **40**, 7687–7693.

74 A. J. Campbell, D. D. C. Bradley and D. G. Lidzey, Space-charge limited conduction with traps in poly(phenylenevinylene) light emitting diodes, *J. Appl. Phys.*, 1997, **82**, 6326–6342.

75 H. Böttger and U. V. Bryskin, *Hopping Conduction in Solids*, Verlag Akademie, Berlin, 1985, p. 169.

76 J. C. Dyre and T. B. Schrøder, Universality of ac conduction in disordered solids, *Rev. Mod. Phys.*, 2000, **72**, 873–892.

77 A. K. Roy, K. Prasad and A. Prasad, Piezoelectric, impedance, electric modulus and Ac conductivity studies on $(Bi_{0.5}Na_{0.5})_{0.95}Ba_{0.05}$ TiO_3 ceramic, *Process. Appl. Ceram.*, 2013, **7**, 81–91.

78 G. Horowitz, M. E. Hajlaoui and R. Hajlaoui, Temperature and gate dependence of hole mobility in polycrystalline oligothiophene thin film transistors, *J. Appl. Phys.*, 2000, **87**, 4456–4463.

79 M. Laajimi, A. Jebnouni, M. Chemli, M. Majdoub and R. Ben Chaabane, Optical, dielectric and oxygen sensing properties of an anthracene and carbazole based π-conjugated Schiff base, *Mater. Chem. Phys.*, 2019, **228**, 336–343.

80 S. Nasreen and M. Baczkowski, Polymer Dielectric for Capacitor Applications, *Kirk-Othmer, Ency. Chem.*, 2017.

81 P. Chutia and A. Kumar, Dielectric and Conductivity Relaxation in Poly(3,4-ethylenedioxythiophene) Nanotubes, *Polym. Eng. Sci.*, 2016, 448–457.

82 S. Das and A. Ghosh, Charge Carrier Relaxation in Different Plasticized PEO/PVDF-HFP Blend Solid Polymer Electrolytes, *J. Phys. Chem. B*, 2017, **121**, 5422.

 This journal is © The Royal Society of Chemistry 2020